THE JOURNAL OF BIOLOGICAL CHEMISTRY VOL. 285, NO. 12, pp. 8918–8926, March 19, 2010

Relaxase DNA Binding and Cleavage Are Two Distinguishable Steps in Conjugative DNA Processing That Involve Different Sequence Elements of the *nic* Site*[S]

Received for publication, August 19, 2009, and in revised form, January 8, 2010 Published, JBC Papers in Press, January 8, 2010, DOI 10.1074/jbc.M109.057539

María Lucas[‡1], Blanca González-Pérez[‡2], Matilde Cabezas[‡], Gabriel Moncalian[‡], Germán Rivas[§], and Fernando de la Cruz[‡3]

From the [‡]Departamento de Biología Molecular, Universidad de Cantabria, and Instituto de Biomedicina y Biotecnología de Cantabria, Consejo Superior de Investigaciones Científicas-UC-IDICAN, C. Herrera Oria s/n, 39011 Santander and the [§]Centro de Investigaciones Biológicas, Consejo Superior de Investigaciones Científicas, Ramiro de Maeztu 9, 28040 Madrid, Spain

TrwC, the relaxase of plasmid R388, catalyzes a series of concerted DNA cleavage and strand transfer reactions on a specific site (*nic*) of its origin of transfer (*oriT*). *nic* contains the cleavage site and an adjacent inverted repeat (IR_2). Mutation analysis in the *nic* region indicated that recognition of the IR_2 proximal arm and the nucleotides located between IR_2 and the cleavage site were essential for supercoiled DNA processing, as judged either by *in vitro nic* cleavage or by mobilization of a plasmid containing *oriT*. Formation of the IR_2 cruciform and recognition of the distal IR_2 arm and loop were not necessary for these reactions to take place. On the other hand, IR_2 was not involved in TrwC single-stranded DNA processing *in vitro*. For single-stranded DNA *nic* cleavage, TrwC recognized a sequence embracing six nucleotides upstream of the cleavage site and two nucleotides downstream. This suggests that TrwC DNA binding and cleavage are two distinguishable steps in conjugative DNA processing and that different sequence elements are recognized by TrwC in each step. IR_2-proximal arm recognition was crucial for the initial supercoiled DNA binding. Subsequent recognition of the adjacent single-stranded DNA binding site was required to position the cleavage site in the active center of the protein so that the *nic* cleavage reaction could take place.

Bacterial conjugation is an efficient and sophisticated DNA transport mechanism, genetically encoded by self-transmissible plasmids. The transfer of DNA by bacterial conjugation plays an important role in the genetic variability of bacteria as well as in the propagation of antibiotic resistance and virulence factors (1). In order to avoid the spread of antibiotic resistance genes via bacterial conjugation, one promising strategy is the use of anti-conjugation-based antimicrobial agents (2, 3). Our group identified unsaturated fatty acids as conjugation inhibitors (4). Their target is unknown, although membrane-associated ATPases could be good candidates. Because the relaxase is the key catalytic enzyme in the conjugative process, it is, *a priori*, a better target for a specific inhibitor. Potts *et al.* (5) found that bisphosphonates inhibited the activity of plasmid F relaxase TraI. Their effect on conjugation inhibition was small, although, surprisingly, they could specifically kill relaxase-containing cells. Moreover, bacterial relaxases might find a use as tools for site-specific DNA delivery to target eukaryotic cells for gene therapy (6). Thus, a detailed study of the specificity determinants of the reaction performed by relaxases could lead to the *a la carte* design of relaxases able to act on any potentially interesting sequence (7).

Conjugative DNA processing is carried out by the relaxosome, composed by the enzyme relaxase and auxiliary proteins that act on the *oriT* region (see Ref. 8 for a review). It starts by a site- and strand-specific DNA cleavage reaction that occurs at a specific *oriT* site called *nic*. The *nic* cleavage reaction is mediated by a tyrosine residue that catalyzes a transesterification reaction. After cleavage, the relaxase remains covalently bound to the 5′-end of the cleaved strand via a phosphotyrosyl linkage, whereas the 3′-hydroxyl is sequestered by tight non-covalent interaction with the relaxase. The cleavage reaction is reversible because the free DNA 3′-hydroxyl group can attack the 5′-phosphotyrosyl bond. However, when the relaxase-DNA complex releases the 3′-OH portion of the DNA (as when it is transported to the recipient cell), a second tyrosine can attack a second *nic* site positioned at the protein active site. This type of reaction takes place at the end of conjugation for regenerating the *oriT* in the recipient cell, and it is known as strand transfer reaction (9, 10).

TrwC is a multidomain protein of 966 amino acids that forms dimers in solution (11). The N-terminal part of the protein contains the relaxase domain (amino acids 1–300) (12), whereas the C-terminal region (amino acids 192–966) is responsible for dimerization and DNA-helicase activity, required for unwinding the transferring DNA (13, 14). TrwC specifically nicks *oriT*-containing supercoiled plasmids *in vitro* in the absence of accessory proteins and remains covalently bound to the 5′-end of the cleaved DNA strand (15). The nicking activity of TrwC allows intermolecular site-specific recombination between two plasmids containing *oriT* in the absence of conjugation (13). Two specific tyrosyl residues in TrwC,

* This work was supported by Spanish Ministry of Education Grants BFU2008-00995/BMC and CIT-010000-2008-4.

[S] The on-line version of this article (available at http://www.jbc.org) contains supplemental Figs. S1 and S2.

[1] Recipient of a predoctoral fellowship from the Public Foundation "Marqués de Valdecilla." Present address: Dept. of Chemistry and Biochemistry, Gene Center, University of Munich, Feodor-Lynen-Str. 25, 81377 Munich, Germany.

[2] Present address: Dept. of Biochemistry, University of Cambridge, 80 Tennis Court Rd., Cambridge CB2 1GA, United Kingdom.

[3] To whom correspondence should be addressed. Tel.: 34-942-201942; Fax: 34-942-201945; E-mail: delacruz@unican.es.

Tyr^{18} and Tyr^{26}, are involved in the DNA strand transfer reactions (9, 10, 12). Tyr^{18} catalyzes the first strand cleavage, whereas Tyr^{26} is involved in the strand transfer reaction that terminates the DNA processing. Between these two steps in conjugation, the DNA strand that was first cleaved is displaced by the helicase activity of TrwC. Similar reactions occur during processing of F plasmid *oriT* by the related relaxase TraI_F. The relaxases of F and R100 plasmids also act as bifunctional relaxases, with relaxase and helicase domains in the same protein (16–18).

Conjugative and mobilizable plasmids of the same MOB family show conservation of the DNA sequence of *oriT* (19, 20). Nevertheless, the *oriT* sequences specifically involved in the so-called initiation and/or termination reactions are unknown for the vast majority of plasmids. The initiation reaction is the first cleavage reaction performed by Tyr^{18} in TrwC. The termination reaction is the second cleavage and strand transfer reaction performed by Tyr^{26} in TrwC. In most analyzed *oriT* regions, an inverted repeat (IR, named IR_2 in R388) is located upstream the *nic* site (20, 21), which is recognized either by the relaxase or by some auxiliary relaxosomal protein (8). The proximal arm of the IR and the region surrounding the *nic* site are sufficient for the initiation reaction in plasmids R64 and R1162, whereas a larger DNA substrate that includes the complete IR is required in the termination reaction. Conversely, in F plasmid, initiation demands a larger DNA substrate than the termination reaction (22).

The three-dimensional crystal structure of the relaxase domain of TrwC ($TrwC_R$) has been solved in complex with its cognate 25-base oligonucleotide substrate, folded in a DNA hairpin (23). The DNA is firmly held by the relaxase by two identifiable binding sites. The hairpin forms an almost perfect B-DNA that is bound by two different motifs through its major and minor grooves. The *nic*-proximal ssDNA[4] is housed in a deep narrow cleft that contains the relaxase catalytic site. Nucleotides involved in that "frozen" interaction with the relaxase were established, but the three-dimensional structure could not reveal which nucleotides participate in the enzymatic reactions of cleavage and strand transfer. In this work, we characterize the biochemical and biophysical properties of the TrwC-DNA complex. In addition, we study the elements involved in DNA sequence recognition in the independent reactions catalyzed by TrwC during conjugative DNA processing. We present evidence that TrwC recognizes its target *nic* region in two steps: an initial scDNA binding involving the proximal arm of IR_2, followed by recognition of the adjacent ssDNA binding site that situates the cleavage site in the right position to be cleaved.

EXPERIMENTAL PROCEDURES

Bacterial Strains, Plasmids, and Oligonucleotides—*Escherichia coli* K12 strains used were DH5α (*F⁻, endA1 recA1 gyrA96 thi-1 hsdR17 supE44 relA1*Δ (*argF⁻ lacZYA*) U169 *ϕ80d lacZ* Δ*M15 gyrA96*) (24), YJ1020 (*lon-510* Δ*arg malPp::I^q rspL*) (25), and C43(DE3) (*F^- dcm ompT hsdS (r_B^- m_B^-) gal* λ (DE3)) (26). Plasmids used are listed in Table 1, together with details of their construction. Oligonucleotides were purchased from MWG and are listed in Table 2.

Protein Purification—For $TrwC_R$ purification, plasmid pSU1588 was used, and the *E. coli* BL21 derivative strain C43-DE3 was

[4] The abbreviations used are: scDNA, supercoiled DNA; ssDNA, single-stranded DNA; dsDNA, double-stranded DNA.

TABLE 1
Plasmids

Variants of plasmid R388 *oriT* were constructed from plasmid pSU4910, which contains a fully functional R388 *oriT* segment of 264 bp (GenBank™ accession number X51505.1, coordinates 59–322). Primers orit322EcoRI and oriTR388HindIII were used to PCR-amplify the *oriT* segment of plasmid pSU1186. The amplified product was digested with EcoRI and HindIII and cloned at the equivalent sites of plasmid pSU18, resulting in plasmid pSU4910. Plasmids with mutant *oriT* were built using the megaprimer site-directed mutagenesis method (43). A first PCR was carried out on template pSU1186 with primer oriTR388HindIII and the oligonucleotide with the desired mutation (either R(12 + 18)mut28–29, R(12 + 18)mut26–27, Rm(23/25), Rm(20/22), Rm(18/19), Rm(13/16), Rm(8/11), Rm(IR), Rm(4/7), or Rm(17)) to obtain plasmids pSU1671, pSU1672, pSU1673, pSU1674, pSU1675, pSU1676, pSU1677, pSU1678, pSU1679, and pSU1680, respectively). The resulting PCR products together with oligonucleotide oriT322EcoRI were used as primers for a second PCR using pSU1186 as template. This fragment, digested with EcoRI and HindIII, was cloned in pSU18 digested with EcoRI and HindIII. Ligation products were used to transform *E. coli* strain DH5α. The identities of all plasmids were verified by DNA sequencing.

Plasmid	Description	Phenotype	Size	Reference/Source
pET3a	Expression vector	Ap^R, Rep(pMB8)	4.6	Ref. 42
pSU1186	pUC8::*oriT* (R388)	Ap^R, Rep(pMB8)	3.1	Ref. 34
pSU1501	pKK223–3::*trwC*	Ap^R, Rep(pMB8)	7.7	Ref. 11
pSU1588	pET3a:: $trwC_R$	Ap^R, Rep(pMB8)	5.5	Ref. 9
pSU1671	pSU18::*oriT* mut28–29	Cm^R, Rep(p15A)	4.9	This work
pSU1672	pSU18::*oriT* mut26–27	Cm^R, Rep(p15A)	4.9	This work
pSU1673	pSU18::*oriT* mut23–25	Cm^R, Rep(p15A)	4.9	This work
pSU1674	pSU18::*oriT* mut20–22	Cm^R, Rep(p15A)	4.9	This work
pSU1675	pSU18::*oriT* mut18–19	Cm^R, Rep(p15A)	4.9	This work
pSU1676	pSU18::*oriT* mut13–16	Cm^R, Rep(p15A)	4.9	This work
pSU1677	pSU18::*oriT* mut8–11	Cm^R, Rep(p15A)	4.9	This work
pSU1678	pSU18::*oriT* mutIR	Cm^R, Rep(p15A)	4.9	This work
pSU1679	pSU18::*oriT* mut4–7	Cm^R, Rep(p15A)	4.9	This work
pSU1680	pSU18::*oriT* mut17	Cm^R, Rep(p15A)	4.9	This work
pSU2007	Km^R derivative of R388	$Km^R Tp^R$IncWTra$^+$	32.0	Ref. 35
pSU4910	pSU18::*oriT* (R388)	Cm^R, Rep(p15A)	4.9	This work

TABLE 2
Oligonucleotides

Name	Oligonucleotide sequence[a]
TrwCNdeI	TCACTCATATGCTCAGTCACATGGTATTGACC
TrwC293END	GGGGGATCCTTAGCTGAAATCTATGCCG
oriT322EcoRI	GGCGAATTCGTAGTGTTACTGTAGTGG
oriTR388HindIII	TGCATCATTGAAGCTTGATAACCCAATG
R(12 + 18)mut26–27	TGCGTATTGTCTCGAGCCCAGATTTAAGGA
R(12 + 18)mut28–29	TGCGTATTGTCTATCTCCCAGATTTAAGGA
R(35 + 8)mutIR	AATGACTTACGGCGTGGGAAACCACGCTATTGTCTATAGCCCA
R388–33comp	TGGGCTATAGACAATACGCACCTTTCGGTGCGC
R46nic(31 + 8)	ATAGCGTGATTTATGCCGCTGCGTTAGGTGT ↓ ATAGCAGG
Fnic(29 + 10)	CAGCAAAAACTTGTTTTTGCGTGGGGTGT ↓ GGTGCTTTTG
R(35 + 8)	AATGACTTACGCGCACCGAAAGGTGCGTATTGTCT ↓ ATAGCCCA
R(25 + 8)	GCGCACCGAAAGGTGCGTATTGTCT ↓ ATAGCCCA
R(22 + 11)	CACCGAAAGGTGCGTATTGTCT ↓ ATAGCCCAGAT
R(19 + 14)	CGAAAGGTGCGTATTGTCT ↓ ATAGCCCAGATTTA
R(16 + 17)	AAGGTGCGTATTGTCT ↓ ATAGCCCAGATTTAAGG
R(12 + 18)	TGCGTATTGTCT ↓ ATAGCCCAGATTTAAGGA
R(14 + 4)	GGTGCGTATTGTCT ↓ ATAG
R(12 + 4)	TGCGTATTGTCT ↓ ATAG
R(6 + 4)	TTGTCT ↓ ATAG
R(25 + 4)	GCGCACCGAAAGGTGCGTATTGTCT ↓ ATAG
R(25 + 0)	GCGCACCGAAAGGTGCGTATTGTCT ↓
R(25-3)	GCGCACCGAAAGGTGCGTATTG
R(25-6)	GCGCACCGAAAGGTGCGTA
Rm(28-29)	GCGCACCGAAAGGTGCGTATTGTCT ↓ AT**CT**CCCA
Rm(26-27)	GCGCACCGAAAGGTGCGTATTGTCT ↓ **CG**AGCCCA
Rm(23-25)	GCGCACCGAAAGGTGCGTATTG**GAG** ↓ ATAGCCCA
Rm(20-22)	GCGCACCGAAAGGTGCGTA**GGC**TCT ↓ ATAGCCCA
Rm(18-19)	GCGCACCGAAAGGTGCG**GC**TTGTCT ↓ ATAGCCCA
R3m(17)	GCGCACCGAAAGGTGC**C**TATTGTCT ↓ ATAGCCCA
Rm(13-16)	GCGCACCGAAA**GTGTA**GTATTGTCT ↓ ATAGCCCA
Rm(8-11)	GCGCACC**TCCC**GGTGCGTATTGTCT ↓ ATAGCCCA
Rm(4-7)	GCG**ACAA**GAAAGGTGCGTATTGTCT ↓ ATAGCCCA
Rm(IR)	G**GCGTGG**GAAA**CCACGC**TATTGTCT ↓ ATAGCCCA

[a] The sequence that corresponds to the inverted repeat IR_2 of R388 *nic* is underlined. Nucleotides that are different from R388 wild type sequence are shown in boldface type. The downward arrow indicates the position of the *nic* cleavage site.

employed as overexpression host. $TrwC_R$ was purified as described (27) and stored at −80 °C.

Sedimentation Equilibrium—The experiments were performed in a Optima XL-A analytical ultracentrifuge (Beckman-Coulter) equipped with absorbance optics, using an An50Ti rotor. $TrwC_R$ (ranging in concentration from 0.1 to 10 μM) in 10 mM Tris-HCl, pH 7.6, 110 mM NaCl, 0.02 mM EDTA was centrifuged at sedimentation equilibrium using short columns (70 ml) at two successive speeds (13,000 and 15,000 rpm) in the absence or in the presence of 1.5 μM oligonucleotide R(25 + 0) (Table 2). The equilibrium scans were taken at 20 °C and three wavelengths (250, 255, and 280 nm) using either standard 12-mm double sector or six-channel centerpieces of charcoal-filled Epon. High speed sedimentation was conducted afterward for base line correction. Cell average molar masses were determined by fitting a sedimentation equilibrium model for a single sedimenting solute to individual data sets with the programs XLAEQ and EQASSOC (supplied by Beckman; see Ref. 28). The partial specific volume of the oligonucleotide was taken as 0.55 ml/g, and the corresponding one of the protein was 0.727 ml/g at 20 °C, calculated from the amino acid composition of the TrwC fragment (13) using the program SEDNTERP (29).

Sedimentation Velocity—Experiments were carried out at 50,000 rpm and 20 °C in the same XL-A instrument, using 12-mm double-sector centerpieces. Apparent sedimentation coefficients were calculated using the programs SVEDBERG (30) and SEDFIT (31), which gave comparable results. The latter program was used to generate apparent sedimentation coefficient distributions, g*(s), by least squares boundary modeling of sedimentation velocity data (32).

Electrophoretic Mobility Shift Assay—$TrwC_R$ binding to the oligonucleotides listed in Fig. 1 and Table 2 was analyzed by an electrophoretic mobility shift assay. Binding reactions contained 1 nM radiolabeled oligonucleotide, 1 μM competitor oligonucleotide, and increasing concentrations of $TrwC_R$ in buffer A (10 mM Tris-HCl, pH 7.6, 110 mM NaCl, 0.02 mM EDTA). The competitor oligonucleotide was a mixture of the following three non-labeled oligonucleotides: 5′-CCAGGTACCTGAGCTGGCCGAAAA, 5′-GCATGCGGATCCGTCGACCTGCAGGG, and 5′-CCAGGATCCCCTTCACGCGATTGGAGCCGT. Reaction mixtures were incubated for 20 min at 20 °C and were loaded onto a 12% non-denaturing polyacrylamide gel. Binding constants were calculated as described before (27). Binding assays with the oligonucleotides listed in Fig. 3 were performed in the same conditions as described before but using a lower concentration of NaCl (50 mM instead of 110 mM).

Oligonucleotide Cleavage and Strand Transfer Assays—Cleavage reaction mixtures contained 50 nM fluorescein-labeled oligonucleotide and variable concentrations of protein $TrwC_R$ in 10 mM Tris-HCl, pH 7.6, 5 mM $MgCl_2$, 110 mM NaCl, and 20 μM EDTA. After incubation for 30 min at 37 °C, digestion with 0.6 mg/ml proteinase K and 0.05% (w/v) SDS was carried out for 20 min at 37 °C. For the oligonucleotide strand transfer reactions, after the incubation of 50 nM 3′-fluorescein-labeled R(12 + 18) with 1 μM $TrwC_R$ for 30 min at 37 °C, a 250 nM concentration of R(25 + 8) or the modified mut oligonucleotides (Fig. 3) was added to the reaction mixture. Reactions were incubated for 1 h at 37 °C and then digested with 0.6 mg/ml proteinase K and 0.05% (w/v) SDS. Samples were injected in the capillary system BioFocus®2000 (Bio-Rad). Oligonucleotide separation and quantification were performed as described previously (9, 27).

Supercoiled DNA Nicking Assay—Reaction mixtures (40 μl) contained 10 nM scDNA of plasmid pSU4910 (or each of the mutants) and 300 nM $TrwC_R$ in 10 mM Tris-HCl, pH 7.6, 50 mM NaCl, 0.02 mM EDTA, and 5 mM $MgCl_2$. After incubation for 30 min at 37 °C, 20 μl of the reaction mixtures were digested with 1 mg/ml Proteinase K (Roche Applied Science) in 0.5% (w/v) SDS for 15 min at 37 °C. The other 20 μl were precipitated with KCl in the presence of SDS (33). SDS was added to a final concentration of 0.2% (w/v), and EDTA was added to a final concentration of 10 mM. The samples were heated at 70 °C for 10 min. The subsequent addition of KCl to a final concentration of 100 mM followed by 15-min incubation at 0 °C induced SDS-KCl precipitation. Separation was carried out by centrifugation at 4 °C for 15 min in a microcentrifuge. The supernatant was removed, and the pellet was resuspended in 20 μl of 10 mM Tris-HCl, pH 8.0, 1 mM EDTA. Reaction mixtures were applied to 0.8% (w/v) agarose gels containing 0.5 μg/ml ethidium bromide and electrophoresed at 100 V in 45 mM Tris borate, 0.5 mM EDTA buffer (pH 8.2). Bands were visualized in a Bio-Rad Gel Doc system and quantified using Quantity One software.

Conjugation Experiments—Conjugation experiments were carried out by the plate-mating procedure as described (34). Derivatives of DH5α containing plasmid pSU2007 (a K_m^R derivative of R388 (35)) and a second plasmid contributing R388-*oriT* (the wild type *oriT* or each of the mutants when indicated) were mated with strain UB1637. Conjugation frequencies were expressed as the number of transconjugants/donor cell.

RESULTS

TrwC nic Cleavage Activity on Single-stranded DNA—$TrwC_R$ cleaves oligonucleotides containing the *nic* site, resulting in two products that can be analyzed by capillary electrophoresis. Experiments were carried out with protein $TrwC_R$, which lacks the helicase domain, to avoid nonspecific interactions between oligonucleotides and the helicase. $TrwC_R$ cleaves both ssDNA and scDNA substrates containing *nic* as efficiently as full-length TrwC (9) and therefore is suitable for binding and *nic* cleavage analysis.

A series of oligonucleotides that varied in the number of nucleotides 5′ and 3′ to *nic* (Fig. 1 and Table 2) were used to map the sequence that is essential for the *nic* cleavage reaction. Cleavage was carried out by incubating each oligonucleotide with increasing concentrations of $TrwC_R$ and digesting the protein that remains covalently attached to the oligonucleotide to release the two cleavage products. These products were subjected to capillary electrophoresis under the conditions described under "Experimental Procedures." There was always a molar excess of protein to guarantee that all of the oligonucleotide is complexed with the protein. To compare the different cleavage ratios, we used 5 μM $TrwC_R$, which allowed saturation in cleavage for all of the samples. Fig. 1 shows the dissociation

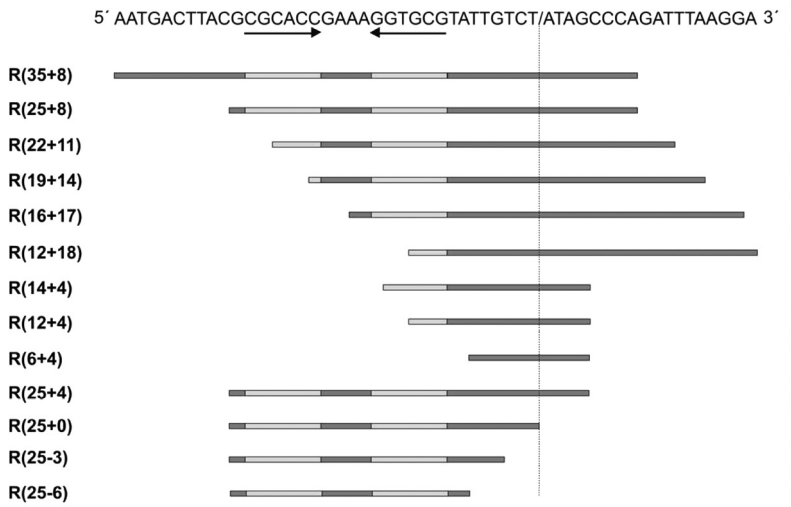

Kd (nM)	nic (%)
34 ± 5	17 ± 1
66 ± 8	10 ± 2
77 ± 10	15 ± 2
134 ± 17	62 ± 3
270 ± 25	83 ± 5
>2000	93 ± 3
320 ± 31	31 ± 1
>2000	34 ± 2
>2000	20 ± 2
84 ± 7	12 ± 2
70 ± 12	n.a
167 ± 22	n.a
482 ± 37	n.a

FIGURE 1. **TrwC-mediated cleavage of oligonucleotides embracing the R388 *nic* site.** The figure shows the dissociation constant (K_d) and percentage cleavage (*nic*) of the oligonucleotides represented *below* the sequence by *horizontal lines*. The values shown are the averages of at least three independent experiments. The DNA sequence of the R388 *nic* site is shown at the *top*. The inverted repeat IR_2 is symbolized by *horizontal arrows below* the DNA sequence. The *nic* site is represented by a *slash* in the sequence. K_d and percentage of cleavage for each oligonucleotide are represented in the *right columns*. *n.a.*, not applicable. Most of the dissociation constants were published previously (23), but they are included in the figure for clarity.

constants and *nic* cleavage activity of $TrwC_R$ using different oligonucleotides ranging from 6 to 35 nucleotides 5′ of the *nic* site and from 0 to 18 nucleotides 3′ of the *nic* site. Oligonucleotides R(12 + 18), R(12 + 4), and R(6 + 4) did not form complexes with $TrwC_R$ in the analyzed concentration range. Nevertheless, $TrwC_R$ was able to efficiently cleave these oligonucleotides at the same protein concentrations (Fig. 1). In fact, oligonucleotides with the highest *nic* cleavage activity turned out to be R(12 + 18) (93%), R(16 + 17) (83%), and R(19 + 14) (62%), all of them with poor binding constants; moreover, a tendency to increase *nic* cleavage efficiency correlated with a reduction of the length of the sequence located 5′ of the cleavage site (from nucleotide 25 to 12) if the sequence 3′ to the cleavage site was longer than 7 nucleotides (Fig. 1). In the same way, an inverse relationship between binding and nicking efficiency was observed. Oligonucleotides R(35 + 8), R(25 + 8), and R(25 + 4) showed the highest binding constants ($K_d < 100$ nM), but poor cleavage. Decreased binding was observed for oligonucleotides R(25-6) and R(25-3) compared with R(25-0) (23), despite the fact that all three oligonucleotides contained a perfect IR_2. Oligonucleotides from related plasmids, like Fnic(29 + 10) and R46nic(31 + 8), or oligonucleotide R388-33comp (Table 2), containing the complementary strand of plasmid R388 *nic*, were not cleaved at all. No cleaved product was observed with these oligonucleotides even at high (10 μM) $TrwC_R$ concentration (data not shown).

Biochemical Characterization of TrwC-DNA Complex—Guasch *et al.* (23) determined the crystal structure of the complex formed by $TrwC_R$ and oligonucleotide R(25 + 0). This structure showed a 1:1 complex. This result was in apparent contradiction with a previous observation that TrwC was a dimer in solution (11). Moreover, the transposase TnpA of insertion sequence IS608, which exhibits a common structural topology with TrwC relaxase domain, was shown to act as a dimer (36, 37). Thus, it seemed important to elucidate if the structure of $TrwC_R$-R(25 + 0) showed the physiological stoichiometry of the complex in solution.

To analyze $TrwC_R$ binding to a radiolabeled R(25 + 8) oligonucleotide, electrophoretic mobility shift assays were carried out (see "Experimental Procedures"). $TrwC_R$ binding to this oligonucleotide produced a shifted band (supplemental Fig. S1*A*). Such a complex results from rapid association/dissociation equilibrium, which is achieved in less than 1 min. Increasing the incubation temperature from 20 to 37 °C had little effect on binding affinity (data not shown). By plotting the electrophoretic mobility shift assay data, the dissociation constant of the protein-DNA complex was calculated to be 30 nM (supplemental Fig. S1*B*). The $TrwC_R$-R(25 + 8) complex could be isolated by gel filtration. After high resolution gel filtration column chromatography of the binding mixture, fractions were analyzed by nondenaturating PAGE, and the fluorescent label of the oligonucleotide was detected (see supplemental material). The major peak corresponded to a $TrwC_R$-oligonucleotide complex (supplemental Fig. S2). The complex was stable, with a half-life of 11 h (23).

Sedimentation equilibrium analysis of $TrwC_R$ showed that, under the experimental conditions, the protein sedimented as a single species with average molecular mass 32,900 ± 3,000 Da (Fig. 2*A*), essentially identical to the theoretical monomer mass derived from its sequence (32,924 Da). The protein had no tendency to self-associate in the analyzed concentration range (0.1–10 μM). The sedimentation coefficient of $TrwC_R$ monomer was 2.68 ± 0.05 S (data not shown). From the combined data, a translational frictional coefficient ratio of 1.27 ± 0.07 was calculated, which is compatible with $TrwC_R$ being a globular monomeric protein in solution.

The oligonucleotide R(25 + 0) at 1.5 μM sedimented also as a single species with molar mass 8,300 ± 1,000 Da (Fig. 2*B*), which essentially corresponds to the monomer (8,290 Da), with a sedimentation coefficient of 1.78 ± 0.05 S (Fig. 2*B*, *inset*) and a frictional ratio of 1.36. Upon incubation of oligonucleotide R(25 + 0) with 2.0 μM $TrwC_R$, the mixture sedimented faster (3.91 S), and the equilibrium gradient was steeper (apparent molecular mass 44,000 Da) than the oligonucleotide alone (Fig. 2*B*), which suggested the formation of a 1:1 protein-oligonucleotide complex.

The Specific nic Sequence Required for TrwC Function in Vivo—To analyze in detail the role of specific *nic* nucleotides recognized by TrwC *in vivo*, we carried out site-directed mutagenesis (Fig. 3). Mutations were introduced on plasmid pSU4910, carrying a functional 264-bp *oriT*, systematically changing nucleotides from position 2 to position 29 of the *nic* site (Fig. 3). As summarized in the *first column* of Fig. 3, mutations from posi-

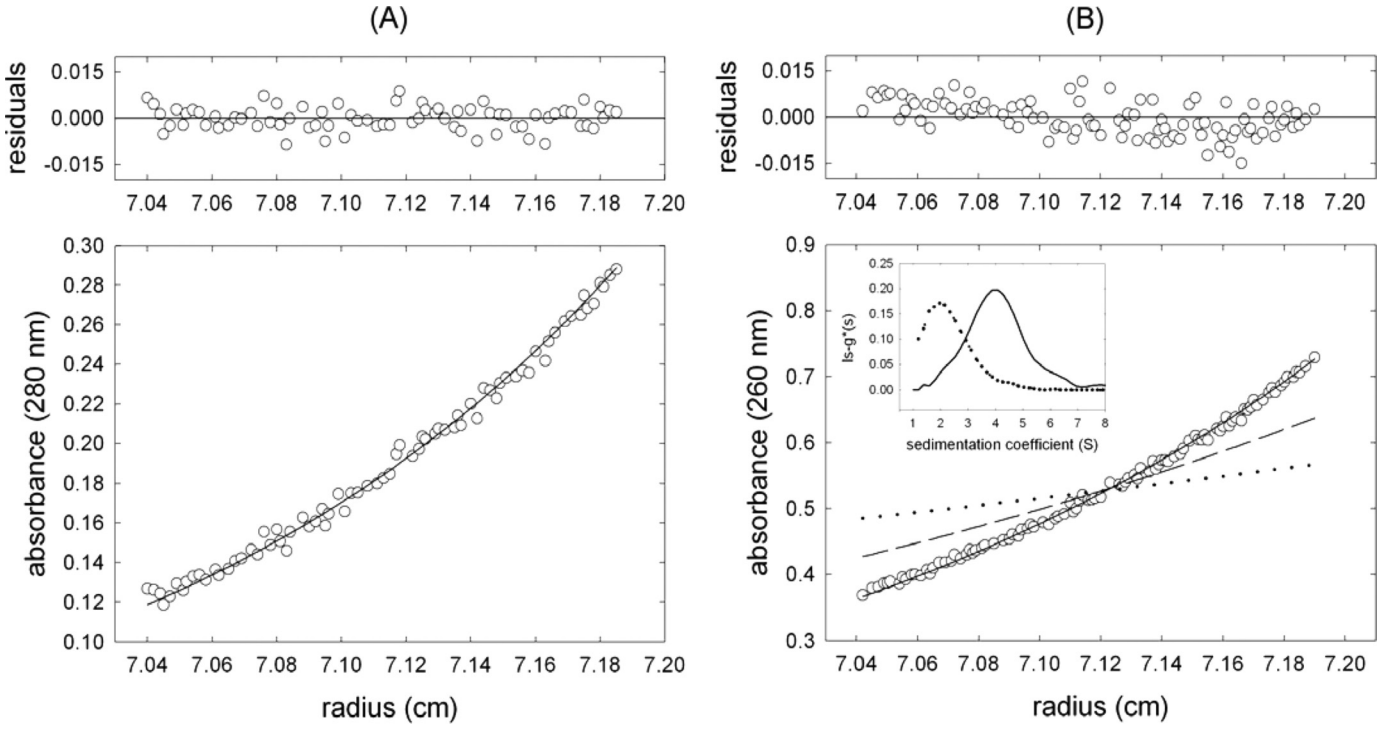

FIGURE 2. **Stoichiometry of $TrwC_R$-R(25 + 0) complexes in solution.** *A*, sedimentation equilibrium gradient (15,000 rpm, 20 °C) of 6 μM $TrwC_R$. The *symbols* represent the experimental data, and the *solid line* shows the best fit gradient, with an average molar mass of 32,900 ± 3,000 Da, which is essentially the monomer mass. *B*, the *symbols* represent the sedimentation equilibrium gradient (13,000 rpm, 20 °C) of a mixture of 2.0 μM $TrwC_R$ with 1.5 μM R(25 + 0) oligonucleotide. The *solid line* is the best fit gradient to a single sedimenting species of 44,000 Da molar mass. For comparative purposes, the theoretical gradients of monomer $TrwC_R$ (*dashed line*) and R(25 + 0) oligonucleotide (*dotted line*) are also shown. *Inset*, apparent sedimentation coefficient distributions, g*(s), at 50,000 rpm and 20 °C for 1.5 μM R(25 + 0) alone (*dashed line*) and in the presence of 2.0 μM $TrwC_R$ (*solid line*).

tion 13 to 27 decreased plasmid mobilization drastically (to 0.04% or less). On the other hand, mutations in the IR_2 loop (nucleotides 8–11) had almost no effect (2-fold), whereas mutations in the distal arm of IR_2 (nucleotides 4–7), which abolish pairing with the proximal arm and would not allow hairpin formation, had quite a small effect on mobilization frequency (10-fold reduction). Conversely, the DNA sequence of the proximal arm of IR_2 seemed to be critical for *oriT* conjugative processing, because mutations in positions 17 and 13–16 dropped mobilization to 0.038 and 0.0002%, respectively. Mutations in both arms of the hairpin (mutIR), which maintained the secondary structure but changed the nucleotide sequence, promoted a drastic reduction of the mobilization frequency (2×10^5-fold). All of these results taken together indicated that the proximal arm was the only essential component of IR_2 for *in vivo* recognition of R388 *nic*, whereas the hairpin structure only slightly improved recognition.

In addition, the 8 nucleotides located between IR_2 and the cleavage site were crucial for mobilization, which decreased 10^5- to 10^6-fold in the *oriT* variants mut18–19, mut20–22, and mut23–25. At the right side of the cleavage site, the first four nucleotides were analyzed. Although the first two nucleotides were found to be essential (mut26–27), mutation of nucleotides 28 and 29 had a relatively small effect (7-fold decrease).

Relaxase Reactions in Vitro on Mutant nic Sites—To complement the data obtained by mobilization, the *oriT* mutants were studied *in vitro* using two types of DNA substrates: scDNA (plasmid DNAs carrying the *oriT* mutations) and ssDNA (33-mer oligonucleotides with the mutations shown in Fig. 3). Mutated *oriT*-containing scDNA was used to test the relaxation ability of the protein on different *oriT* variants, and ssDNA oligonucleotides were used to dissect binding, cleavage, and strand transfer reactions.

Relaxation of scDNA was analyzed as described under "Experimental Procedures," using the same pSU4910 derivatives as those used for mobilization (Fig. 4). Three different outcomes were observed in the relaxation of scDNA by $TrwC_R$-wild type or fully relaxed DNA (mut4–7), partially relaxed DNA (mut8–11 and mut28–29), and non-relaxed DNA (mut13–16, mut17, mut18–19, mut20–22, mut23–25, mut26–27, and mutIR) (see Fig. 4 and the *last column* of Fig. 3). These data indicated that the *in vitro* requirements for scDNA recognition by $TrwC_R$ were the same as those for *in vivo* mobilization. The critical region coincided in both *in vivo* and *in vitro* processes and comprised nucleotides 13–27 (Fig. 3). Furthermore, these results indicate that scDNA processing might be the limiting step in plasmid R388 mobilization.

Electrophoretic mobility shift assays with oligonucleotides (see "Experimental Procedures") allowed the determination of the region that was specifically recognized for $TrwC_R$ binding. High specificity binding to these oligonucleotides required a larger DNA sequence than that needed for scDNA relaxation or *in vivo* mobilization. The region involved was comprised from the cleavage site to the end of the distal arm of IR_2, with the exception of the hairpin loop. The nucleotides located 3′ to the *nic* site seemed not to be specifically recognized for binding (Fig. 3, *column 2*). Thus, high affinity binding is not a basic requirement for mobilization ability.

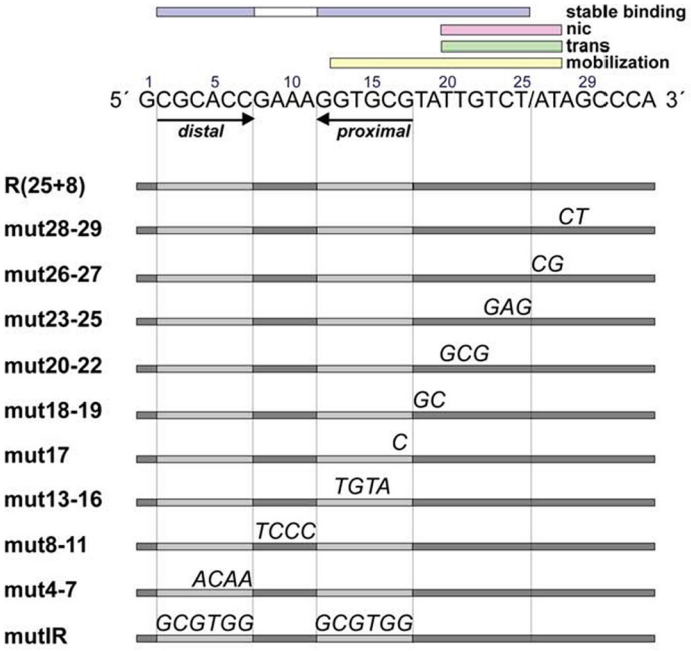

oriT mobilization (conjugation frequencies)	Kd (nM)	nic (%)	trans (%)	relax (%)
$2.9\cdot10^{-2}$ ($1.5\cdot10^{-2}$-$5.7\cdot10^{-2}$)	30 ± 5	27 ± 1	25 ± 1	+++
$4.7\cdot10^{-3}$ ($2.1\cdot10^{-3}$-$1.0\cdot10^{-2}$)	31 ± 9	27 ± 1	12 ± 1	++
$1.5\cdot10^{-6}$ ($5.5\cdot10^{-7}$-$4.2\cdot10^{-6}$)	32 ± 7	0	0	-
$5.0\cdot10^{-8}$ ($3.1\cdot10^{-8}$-$8.2\cdot10^{-8}$)	195 ± 38	0	0	-
$4.4\cdot10^{-8}$ ($2.0\cdot10^{-8}$-$9.7\cdot10^{-8}$)	265 ± 43	0	0	-
$2.8\cdot10^{-7}$ ($7.4\cdot10^{-8}$-$1.1\cdot10^{-6}$)	94 ± 18	84 ± 3	29 ± 2	+
$1.1\cdot10^{-5}$ ($6.4\cdot10^{-6}$-$1.9\cdot10^{-5}$)	71 ± 10	78 ± 1	ND	ND
$4.6\cdot10^{-8}$ ($1.8\cdot10^{-8}$-$1.1\cdot10^{-7}$)	93 ± 4	84 ± 3	25 ± 2	-
$1.6\cdot10^{-2}$ ($6.1\cdot10^{-3}$-$4.4\cdot10^{-2}$)	42 ± 6	17 ± 2	30 ± 2	++
$3.1\cdot10^{-3}$ ($1.7\cdot10^{-3}$-$5.4\cdot10^{-3}$)	88 ± 15	75 ± 3	23 ± 1	+++
$1.4\cdot10^{-7}$ ($2.6\cdot10^{-8}$-$7.5\cdot10^{-7}$)	>1000	42 ± 5	11 ± 1	-

FIGURE 3. **Analysis of TrwC binding site by mutagenesis.** The DNA sequence of the R388 *nic* site is shown at the *top*. A *slash* in the sequence indicates the position of the *nic* cleavage site. The *horizontal bars* represent the oligonucleotides named in the *left column*. Mutant nucleotides are indicated *above* the *horizontal bar*. For the mobilization experiments, derivatives of strain DH5α containing plasmid pSU2007 plus either pSU4910 or any of its mutants (Table 1) were mated with strain UB1637, and transconjugants were selected as explained under "Experimental Procedures." Mobilization frequencies (*column 1*) were calculated as the number of transconjugants (Cm^RNx^R) divided by the number of donors (Cm^RSm^R). The first value corresponds to the mean value, whereas S.D. values (assuming a log-normal distribution) appear in *parentheses*. The values are averages of five independent experiments. K_d, dissociation constants calculated with the binding data, as represented in Fig. 1, by non-linear regression fit of the data using GraphPad Prism™ 3.02. % *nic*, cleavage ratio at 1 μM $TrwC_R$. *ND*, not determined. The nucleotides within the extension that are critical for mobilization (*yellow*), TrwC binding (*blue*), *nic* cleavage (*pink*), and strand transfer (*green*) are marked with a *box over* the DNA sequence.

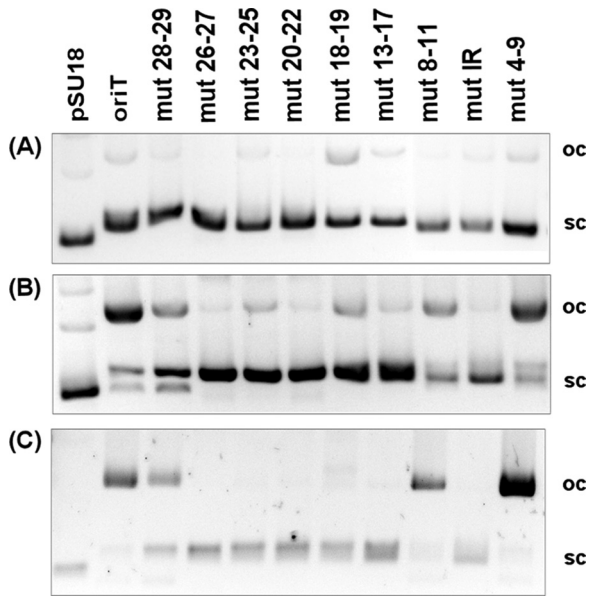

FIGURE 4. **Relaxation reaction of protein $TrwC_R$ with different plasmid DNAs containing mutant *oriTs*.** *A*, 20 μl of plasmids (10 nM). *Lane 1*, pSU18; *lane 2*, pSU4910; *lane 3*, pSU1671 (mut28–29; *lane 4*, pSU1672 (mut26–27); *lane 5*, pSU1673 (mut23–25); *lane 6*, pSU1674 (mut20–22); *lane 7*, pSU1675 (mut18–19); *lane 8*, pSU1676 (mut13–17); *lane 9*, pSU1677 (mut8–11); *lane 10*, pSU1678 (mutIR); *lane 11*, pSU1679 (mut4–7). *B*, relaxation products of the same plasmids as in *A*. $TrwC_R$ (300 nM) was incubated with DNA (10 nM) in the presence of 10 mM Tris, pH 7.6, 50 mM NaCl, 0.02 mM EDTA, and 5 mM $MgCl_2$ for 30 min at 37 °C. Then the reaction mixture was digested with proteinase K. *C*, DNA-protein covalent complex precipitation in the presence of KCl. The *lanes* correspond to the plasmids indicated in *A*. *sc*, supercoiled; *oc*, open circle.

Finally, cleavage and strand transfer of ssDNA oligonucleotides did not require IR_2 and occurred efficiently with oligonucleotides containing wild type positions 20–27 (see Fig. 3, *column 3*). Remarkably, mutations in positions 13–19 resulted in increased cleavage, suggesting that these positions were important for complex stability. In all cases, the *nic* cleavage products corresponded to the length expected for cleavage at the canonical site (data not shown).

DISCUSSION

The interaction between a conjugative relaxase and its target site is the initial step for conjugative DNA processing. Recognition of the *nic* site has to be specific enough so that a single sequence can be selected out of a complete bacterial genome (in fact out of a number of genomes of potential bacterial hosts). As we show in this paper, this exquisite recognition is brought about by separating it into two different steps. TrwC binds to a palindromic DNA sequence formed in a double-stranded region of the DNA (binding sequence) and then cleaves in an adjacent sequence if a second specific sequence is found (cleavage sequence). TrwC binding to the palindromic sequence IR_2 was previously defined by protein crystallography. The present results indicate that TrwC binds IR_2 with high affinity. Moreover, the stoichiometry of the complex was found to be a 1:1 molar ratio. This oligomerization state is consistent with the data presented in Ref. 9. Although this perfect palindromic IR was recognized and bound by TrwC with high affinity, shorter oligonucleotides not containing the entire IR were effectively cleaved by TrwC.

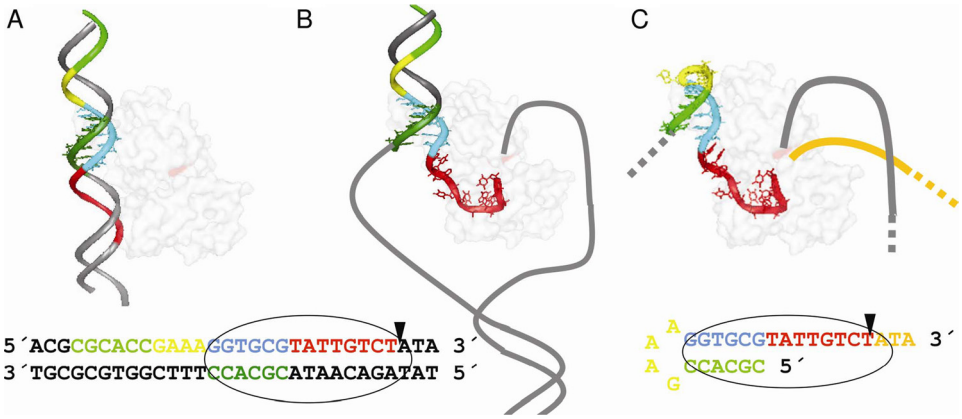

FIGURE 5. **Model of TrwC *oriT* recognition in the conjugation process.** *A*, TrwC (*light shaded element*) recognizes the dsDNA containing the proximal arm of IR_2 (DNA in *sticks representation*) in the donor cell. *B*, high affinity binding to the proximal arm allows local melting of the DNA around the cleavage site and the generation of a U-shaped turn in the transferred ssDNA strand that positions the *nic* site in the TrwC active site. *C*, TrwC recognizes the ssDNA containing both arms of IR_2 in the recipient cell. *Red*, bases T^{20}–T^{25}, which are recognized in the ssDNA processing; *cyan*, additional bases (G^{12}–A^{19}) relevant for scDNA relaxation; *dark green*, complementary sequence of the proximal arm of IR_2; *yellow*, IR_2 loop; *light green*, distal arm of IR_2; *orange*, DNA generated by rolling circle replication. The position of TrwC Tyr^{18} is indicated in *magenta* on the protein surface. The sequence of the dsDNA or ssDNA recognized by TrwC is shown *below* with the same *color code* as in the model.

When binding and cleavage of oligonucleotides R(25 + 4), R(14 + 4), R(12 + 4), and R(6 + 4) were compared, we observed that the absence of the distal repeat of the IR_2 deteriorated TrwC binding ability (Fig. 1). However, *nic* cleavage activity remained intact in the oligonucleotides without the IR_2 distal arm, indicating that IR_2 is dispensable for cleavage but essential for high affinity binding to the relaxase. The relaxase binds these oligonucleotides poorly but sufficiently well to recognize the sequence required for *nic* cleavage. These results suggest that $TrwC_R$ has to recognize one sequence for binding and another for *nic* cleavage, although both are required for proper binding, and both are required for a proper *nic* cleavage.

nic cleavage efficiency was increased by reduction of the length of the sequence located 5′ of the cleavage site (from 25 to 12 nucleotides). In the same way, we observed an inverse relationship between binding and *nic* cleavage efficiency. This apparent contradiction was explained by experiments using suicide nucleotides (9). These nucleotides displaced the reaction equilibrium to the formation of products, therefore reducing the reverse joining reaction. In this way, R(25s + 4) did not show reduced *nic* cleavage activity but rather increased rejoining efficiency, due to better TrwC binding that positions the 3′-OH in a better place to attack the phospho-tyrosyl bond and religate the oligonucleotide. In the same line of thought, we observed that increasing the incubation time produced higher *nic* cleavage yields in all cases. In fact, after 48 h of incubation, all oligonucleotides were cleaved to a similar amount. Therefore, different cleavage yields are due to the different dissociation rates of the cleaved product and not to different recognition or cleavage efficiency. Unstable binding could provoke dissociation of the 5′ product that normally remains captured by the relaxase. Consequently, the equilibrium of the cleavage-joining reaction would be displaced toward the *nic* cleavage products.

To further analyze the role of the different DNA residues in TrwC binding and cleavage, we performed mutagenesis analysis, the results of which are summarized on Fig. 3. According to these results, we can dissect the TrwC binding site in two regions: the IR_2 binding site (comprising the distal and proximal arms) and the single-stranded binding site.

IR_2 Distal Arm—As mentioned above, IR_2 is essential for oligonucleotide binding but not for scDNA cleavage. Thus, mutations in the distal arm, which affect ssDNA but not scDNA binding, only slightly affect mobilization. As expected, binding of the oligonucleotide containing this mutation is impaired but not its cleavage. Strikingly, the mobilizable scDNA was cleaved by TrwC with the same efficiency as wild type *oriT*. These results are surprising, considering that the DNA sequence bound by TrwC starts at −25 according to the three-dimensional structure of the TrwC-*nic* complex. Thus, it seems that the role of the IR_2 distal arm is to allow cruciform formation (that probably only occurs during the termination reaction on the transported T-strand), because specific interactions with TrwC do not play a crucial role.

IR_2 Loop—Mutations in the IR_2 loop did not affect substantially any of the properties analyzed (see Rm8–11 results in Fig. 3). This is consistent with TrwC-*nic* crystal structure, where no direct interaction between TrwC and any of the four nucleotides of the loop was observed.

IR_2 Proximal Arm—This segment is essential for mobilization, binding, and cleavage of scDNA (but not ssDNA cleavage). The specific interactions of TrwC with these residues are abundant in the crystal structure. Thus, modification of these residues abrogates $TrwC_R$ binding to this site. $TrwC_R$ recognizes not only the B-DNA form of IR_2 (*i.e.* its proximal arm on dsDNA) but also the nitrogenated bases of the nucleotides forming the IR, as observed in the mutant that changes the nucleotides but maintains an IR at the same position as IR_2. In this case, mobilization and binding activity are both lost. Because the specific sequence of the distal arm or the loop is not essential, but the specific sequence of the hairpin is essential, we can conclude that the interactions of this DNA region with the protein are crucial in the recognition.

These data allow us to present a model for the role of IR_2 in R388 conjugation (Fig. 5). According to this model, TrwC recognizes the dsDNA containing the proximal arm of IR_2 in the donor cell (Fig. 5*A*). This is consistent with the fact that TrwC recognizes and cleaves scDNA containing mutations in the IR_2 distal arm. It is also consistent with the crystal structure of the TrwC-*nic* complex if we understand that the hairpin bound in the structure is a representation of the proximal arm dsDNA bound by the relaxase *in vivo*. In fact, the absence of involvement of the loop in recognition makes a single-stranded cruciform containing the distal and proximal arms of IR_2 indistinguishable from a scDNA containing both strands of the

proximal arm. High affinity binding to the proximal arm allows local melting of the DNA around the cleavage site and the generation of a U-shaped turn in the transferred ssDNA strand that positions the *nic* site in the TrwC active site (Fig. 5*B*). The specific requirements of the nucleotides that form the U-shaped turn will be discussed below. After cleavage, the displaced ssDNA in the donor DNA molecule is transported to the recipient cell being piloted by the relaxase, where the ssDNA is recircularized. In this step, the reaction requires TrwC to recognize the *nic* site after one round of replication. However, because the DNA is transported in a single-stranded form, the new binding site will not be dsDNA this time but ssDNA. It is in this second recognition step that both arms of the IR_2 are needed (Fig. 5*C*).

Analogous results were observed for plasmid R1162 (38), where it was found that mutations in the outer arm of the IR adjacent to *nic* did not affect mobilization. These authors reported that this part of *nic* was involved in the termination reaction.

An interesting result was obtained with the mutants in G^{17}. This nucleotide should interact with its counterpart C^2. Instead, according to the available crystal structures, G^{17} interacts with TrwC residues Arg^{81} and Asp^{183}. Due to this interaction, G^{17} is the first nucleotide of the ssDNA region, and it seems that the interaction of G^{17} with Arg^{81} and Asp^{183} is essential for the extension of the ssDNA segment up to the *nic* site. This structural observation could explain why the mutant oligonucleotide is bound and cleaved by the protein, but nevertheless the corresponding plasmid cannot be mobilized.

Single-stranded Binding Site—Using oligonucleotides lacking IR_2 (R(14 + 4), R(12 + 4), and R(6 + 4)), we observed that IR_2 is dispensable for cleavage but essential for high affinity binding to the relaxase (Fig. 1). The relaxase binds the above oligonucleotides poorly but sufficiently to recognize and cleave the *nic* site. Even oligonucleotide R(6 + 4) seemed to contain enough sequence information to position the scissible phosphate in the catalytic center so that the oligonucleotide could be cleaved.

As observed when binding to oligonucleotides R(25-6), R(25-3), and R(25-0) was compared, the ssDNA binding site also contributes to TrwC stable binding (23). These results suggest that $TrwC_R$ is recognizing two different sequences, one for high affinity binding and a second one for *nic* cleavage.

The effect of the mutations between IR_2 and the *nic* cleavage site corresponded to what could have been predicted from the crystal structure. Inside this core region (nucleotide positions 13–27), two phenotypes could be distinguished. Mutations in the segment from position 20 to 27 resulted in oligonucleotides inactive for cleavage. Nucleotides 20–27 form the U-shaped turn necessary to localize the *nic* site at the catalytic center. Mutations in any of these nucleotides affect the interaction with several residues within the $TrwC_R$ cleft, where the U turn is bound. Moreover, the base interaction between T^{25} and G^{22} stabilizes the U-turn that drives the *nic* site to the close proximity of the catalytic tyrosine. This three-base intrastrand interaction to form the U-turn was also observed in the crystal structure of the TraI relaxase (39, 40).

On the other hand, mutations in the region from 19 to 13 resulted in oligonucleotides that were cleaved with enhanced efficiency. A similar result occurred when oligonucleotide R(12 + 18) was used, suggesting that the lack of appropriate interactions in this region could be affecting (i) the stability of the bound oligonucleotide and thus its off-rate (unlikely because K_d is not grossly affected, and complex half-life is 11 h) or (ii) the positioning of the oligonucleotide with respect to the cleavage site. Perhaps binding to this region is modulating the cleavage efficiency of the protein. In fact, Williams and Schildbach (41) also found that similar mutations in the *nic* site of plasmid F resulted in enhanced cleavage at high relaxase concentration.

In summary, TrwC recognizes dsDNA and specifically binds the proximal arm of IR_2. Upon binding, the bound DNA is distorted so that local DNA melting is created around the *nic* cleavage site, and the DNA can be cleaved by TrwC. For this second step, recognition of specific nucleotides is required to allow the formation of a U-shaped turn that locates the *nic* site at the catalytic center of TrwC. Finally, both the distal and proximal arms of IR_2 are necessary for hairpin formation in the recipient cell. Thus, there are two distinguishable recognition sites, each for a different step of the processing reaction, both required for efficient conjugation. Because all the reported *nic* sites are located between 5 and 10 nucleotides from a more or less perfect inverted repeat (20), we propose that the above mechanism is a general mechanism shared by all of the conjugative relaxases. As a consequence, we hope our results and the two-step model in TrwC target recognition will have an application in the search and characterization of relaxase inhibitors that inhibit plasmid conjugation. In addition, they could help in the design of relaxase variants that can insert in specific genomic sequences, thus providing new tools for genomic engineering.

REFERENCES

1. de la Cruz, F., and Davies, J. (2000) *Trends Microbiol.* **8,** 128–133
2. Filutowicz, M., Burgess, R., Gamelli, R. L., Heinemann, J. A., Kurenbach, B., Rakowski, S. A., and Shankar, R. (2008) *Plasmid* **60,** 38–44
3. Potts, R. G., Lujan, S. A., and Redinbo, M. R. (2008) *Future Microbiol.* **3,** 119–123
4. Fernandez-Lopez, R., Machón, C., Longshaw, C. M., Martin, S., Molin, S., Zechner, E. L., Espinosa, M., Lanka, E., and de la Cruz, F. (2005) *Microbiology* **151,** 3517–3526
5. Lujan, S. A., Guogas, L. M., Ragonese, H., Matson, S. W., and Redinbo, M. R. (2007) *Proc. Natl. Acad. Sci. U.S.A.* **104,** 12282–12287
6. Llosa, M., and de la Cruz, F. (2005) *Res. Microbiol.* **156,** 1–6
7. González-Pérez, B., Carballeira, J. D., Moncalián, G., and de la Cruz, F. (2009) *Biotechnol. J.* **4,** 554–557
8. Zechner, E. L., de la Cruz, F., Eisenbrandt, R., Grahn, A. M., Koraimann, G., Lanka, E., Muth, G., Pansegrau, W., Thomas, C. M., Wilkins, B. M., and Zatyka, M. (2000) in *The Horizontal Gene Pool: Bacterial Plasmids and Gene Spread* (Thomas, C. M., ed) Harwood Academic Publishers, Amsterdam
9. Gonzalez-Perez, B., Lucas, M., Cooke, L. A., Vyle, J. S., de la Cruz, F., and Moncalián, G. (2007) *EMBO J.* **26,** 3847–3857
10. Garcillán-Barcia, M. P., Jurado, P., González-Pérez, B., Moncalián, G., Fernández, L. A., and de la Cruz, F. (2007) *Mol. Microbiol.* **63,** 404–416
11. Grandoso, G., Llosa, M., Zabala, J. C., and de la Cruz, F. (1994) *Eur. J. Biochem.* **226,** 403–412
12. Grandoso, G., Avila, P., Cayón, A., Hernando, M. A., Llosa, M., and de la Cruz, F. (2000) *J. Mol. Biol.* **295,** 1163–1172
13. Llosa, M., Bolland, S., Grandoso, G., and de la Cruz, F. (1994) *J. Bacteriol.*

176, 3210–3217
14. Llosa, M., Grandoso, G., Hernando, M. A., and de la Cruz, F. (1996) *J. Mol. Biol.* **264,** 56–67
15. Llosa, M., Grandoso, G., and de la Cruz, F. (1995) *J. Mol. Biol.* **246,** 54–62
16. Reygers, U., Wessel, R., Müller, H., and Hoffmann-Berling, H. (1991) *EMBO J.* **10,** 2689–2694
17. Matson, S. W. (1991) *Prog. Nucleic Acid Res. Mol. Biol.* **40,** 289–326
18. Fukuda, H., and Ohtsubo, E. (1995) *J. Biol. Chem.* **270,** 21319–21325
19. Garcillán-Barcia, M. P., Francia, M. V., and de la Cruz, F. (2009) *FEMS Microbiol. Rev.* **33,** 657–687
20. Francia, M. V., Varsaki, A., Garcillán-Barcia, M. P., Latorre, A., Drainas, C., and de la Cruz, F. (2004) *FEMS Microbiol. Rev.* **28,** 79–100
21. Parker, C., Becker, E., Zhang, X., Jandle, S., and Meyer, R. (2005) *Plasmid* **53,** 113–118
22. Gao, Q., Luo, Y., and Deonier, R. C. (1994) *Mol. Microbiol.* **11,** 449–458
23. Guasch, A., Lucas, M., Moncalián, G., Cabezas, M., Pérez-Luque, R., Gomis-Rüth, F. X., de la Cruz, F., and Coll, M. (2003) *Nat. Struct. Biol.* **10,** 1002–1010
24. Grant, S. G., Jessee, J., Bloom, F. R., and Hanahan, D. (1990) *Proc. Natl. Acad. Sci. U.S.A.* **87,** 4645–4649
25. Jubete, Y., Maurizi, M. R., and Gottesman, S. (1996) *J. Biol. Chem.* **271,** 30798–30803
26. Miroux, B., and Walker, J. E. (1996) *J. Mol. Biol.* **260,** 289–298
27. Boer, R., Russi, S., Guasch, A., Lucas, M., Blanco, A. G., Pérez-Luque, R., Coll, M., and de la Cruz, F. (2006) *J. Mol. Biol.* **358,** 857–869
28. Minton, A. P. (1994) in *Modern Analytical Ultracentrifugation* (Schuster, T. M., and Laue, T. M., eds) Birkhauser, Boston, MA
29. Laue, T. M., Shah, B. D., Ridgeway, T. M., and Pelletier, S. L. (1992) in *Analytical Ultracentrifugation in Biochemistry and Polymer Science* (Harding, S. E., Rowe, A. J., and Horton, J. C., eds) Royal Society of Chemistry, Cambridge, UK
30. Philo, J. S. (1997) *Biophys. J.* **72,** 435–444
31. Schuck, P. (1998) *Biophys. J.* **75,** 1503–1512
32. Schuck, P., and Rossmanith, P. (2000) *Biopolymers* **54,** 328–341
33. Trask, D. K., DiDonato, J. A., and Muller, M. T. (1984) *EMBO J.* **3,** 671–676
34. Llosa, M., Bolland, S., and de la Cruz, F. (1991) *Mol. Gen. Genet.* **226,** 473–483
35. Martinez, E., and de la Cruz, F. (1988) *Mol. Gen. Genet.* **211,** 320–325
36. Barabas, O., Ronning, D. R., Guynet, C., Hickman, A. B., Ton-Hoang, B., Chandler, M., and Dyda, F. (2008) *Cell* **132,** 208–220
37. Guynet, C., Hickman, A. B., Barabas, O., Dyda, F., Chandler, M., and Ton-Hoang, B. (2008) *Mol. Cell* **29,** 302–312
38. Becker, E. C., and Meyer, R. J. (2000) *J. Mol. Biol.* **300,** 1067–1077
39. Datta, S., Larkin, C., and Schildbach, J. F. (2003) *Structure* **11,** 1369–1379
40. Hekman, K., Guja, K., Larkin, C., and Schildbach, J. F. (2008) *Nucleic Acids Res.* **36,** 4565–4572
41. Williams, S. L., and Schildbach, J. F. (2006) *Nucleic Acids Res.* **34,** 426–435
42. Rosenberg, A. H., Lade, B. N., Chui, D. S., Lin, S. W., Dunn, J. J., and Studier, F. W. (1987) *Gene* **56,** 125–135
43. Sarkar, G., and Sommer, S. S. (1990) *BioTechniques* **8,** 404–407